ISSN 1063-7745, Crystallography Reports, 2020, Vol. 65, No. 2, pp. 269–277. © Pleiades Publishing, Inc., 2020.
Russian Text © The Author(s), 2020, published in Kristallografiya, 2020, Vol. 65, No. 2, pp. 271–280.

STRUCTURE OF MACROMOLECULAR COMPOUNDS

X-Ray Structure and Molecular Dynamics Study of Uridine Phosphorylase from *Vibrio cholerae* in Complex with 2,2'-Anhydrouridine

P. A. Eistrikh-Heller[a], S. V. Rubinsky[a], I. I. Prokofev[a], A. G. Gabdulkhakov[a], A. S. Mironov[b], and A. A. Lashkov[a,*]

[a] *Shubnikov Institute of Crystallography of Federal Scientific Research Centre "Crystallography and Photonics," Russian Academy of Sciences, Moscow, 119333 Russia*

[b] *State Research Institute of Genetics and Selection of Industrial Microorganisms of the National Research Center "Kurchatov Institute," Moscow, 117545 Russia*

**e-mail: alashkov83@gmail.com*

Received June 17, 2019; revised June 17, 2019; accepted August 29, 2019

Abstract—The high-resolution three-dimensional structure of uridine phosphorylase from the pathogenic bacterium *Vibrio cholerae* in complex with the competitive inhibitor 2,2'-anhydrouridine was determined by X-ray diffraction (RCSBPDB ID: 6RCA). The three-dimensional structure of this complex is compared with the previously determined structures of *V. cholerae* uridine phosphorylase in complex with the substrate (uridine) and *S. typhimurium* uridine phosphorylase in complex with 2,2'-anhydrouridine. The protein–inhibitor and protein–substrate binding free energies were calculated by the free-energy perturbation method. The number of stable hydrogen bonds between the 2,2'-anhydrouridine molecule and the active site of the enzyme is smaller and these bonds are longer compared to the natural substrate of the enzyme (uridine). However, calculations taking into account solvation energy of the molecule and the entropy effects showed that the binding of the inhibitor (2,2'-anhydrouridine) at the active site of the protein is energetically more favorable than the binding of the native substrate (uridine). These results may be useful in the design of new inhibitors with a higher selectivity for the binding sites of uridine phosphorylases.

DOI: 10.1134/S1063774520020066

INTRODUCTION

In many types of human tumor cells, the demand for pyrimidine nitrogenous bases increases during the disease development, thereby raising expression levels of uridine phosphorylase (UPh). This enzyme catalyzes the phosphorolytic cleavage of pyrimidine nucleosides and the reverse nucleoside synthesis from (deoxy)ribose 1-phosphate and nitrogenous bases [1–5]. Therefore, the cancer treatment uses pharmacological agents that affect metabolism of nitrogenous bases and their derivatives. In particular, UPh inhibitors are such agents. These inhibitors have strong antiparasitic and antimicrobial activity, because a thymidine-selective enzyme required for the thymidine resynthesis [6] is absent in most protozoans as opposed to mammals.

Currently, the developed UPh inhibitors (except for phosphanes) are various pyrimidine base derivatives. A decrease in concentration of these inhibitors leads to the restoration of UPh activity. Therefore, they are reversible competitive inhibitors [7–9].

The design of ligands for uridine phosphorylase as new drugs requires detailed high-resolution X-ray diffraction data on the three-dimensional organization of macromolecular UPh complexes (including those with appropriate inhibitors). Chemical derivatives of 2,2'-anhydrouridine (ANU) were shown to be the most effective inhibitors for the majority of UPhs from bacterial cells [10, 11].

The structure of uridine phosphorylase from *Salmonella typhimurium* (*St*UPh) in complex with ANU was described previously [12–14]. In these studies, modified 2,2'-anhydrouridine-based ligands having higher affinity for both prokaryotic and eukaryotic UPhs were proposed. Here we report the structure of uridine phosphorylase from another bacterial source, namely *Vibrio cholerae*, in complex with ANU determined by X-ray diffraction at 1.34 Å resolution. The three-dimensional structure of this complex is compared with the previously determined structures of *V. cholerae* uridine phosphorylase (*Vch*UPh) in complex with the substrate uridine (URI) and of *S. typhimurium* uridine phosphorylase in complex with 2,2'-anhydrouridine. The complexes were studied by classical molecular dynamics methods. The protein–ligand binding free energy was calculated by the free-

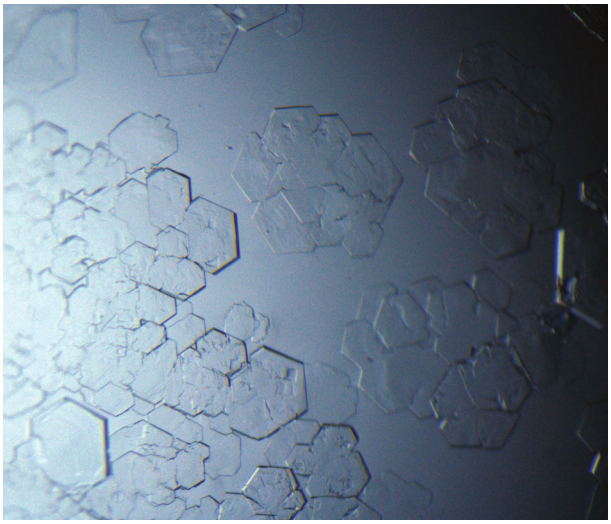

Fig. 1. Crystals of uridine phosphorylase from *V. cholerae* in complex with 2,2'-anhydrouridine.

energy perturbation method. These results can be considered as the basis for chemical modifications of 2,2'-anhydrouridine in the design of new inhibitors of the enzyme with a higher selectivity for the binding sites of both prokaryotic and eukaryotic uridine phosphorylases.

MATERIALS AND METHODS

Isolation and Purification of VchUPh

The enzyme *Vch*UPh was purified by two-step ion-exchange chromatography on butyl-Sepharose and *Q*-Sepharose (Amersham Pharmacia Biotech) in the first and second steps, respectively. According to SDS gel electrophoresis, the homogeneity of the *Vch*UPh specimen was 96%. Procedures for the harvesting of the biomass of the producer, as well as for the isolation and purification of *Vch*UPh were described in [15–17].

Crystallization of VchUPh in Complex with 2,2'-Anhydrouridine

The crystallization was performed by the hanging-drop vapor-diffusion technique at 293 K. The crystallization drops were composed of 1.5 μL of a *Vch*UPh solution with a concentration of 15 mg/mL in tris-HCl buffer, 1.5 μL of the reservoir solution (0.2 M $MgCl_2 \cdot 6H_2O$, 15% (w/v) PEG 4000, 0.1 M tris-HCl, pH 8.5), and 1 μL of a 0.2 M aqueous solution of 2,2'-anhydrouridine. The crystals of the complex (Fig. 1) were grown in one week.

X-ray Diffraction Data Collection and Processing

The experimental X-ray diffraction data set was collected from a crystal of *Vch*UPh in complex with 2,2'-anhydrouridine at the beamline BL14.1 of the BESSY II synchrotron radiation source (Berlin, Germany) at 100 K. The experimental intensities of reflections were processed with the XDS program package [18]. The X-ray data collection and processing statistics are given in Table 1.

Structure Solution and Refinement

The initial phases of the structure factors were obtained by the molecular-replacement method using the Phaser program [19, 20]. The structure of *Vch*UPh in complex with 6-methyluracil (IDPDB: 4K6O) [21] was used as the starting model, from which all ligands, including enzyme-bound water molecules, were removed. The subsequent rigid-body refinement was performed with the phenix.refine program [22, 23] followed by the restrained refinement. The stereochemical parameters of the structural model were visually inspected and the manual rebuilding of the structure was performed with the Coot interactive graphics program [24, 25]. An analysis of σ_A-weighted F_o-F_c and $2F_o-F_c$ electron density maps revealed the position of the inhibitor 2,2'-anhydrouridine in the active site of the enzyme *Vch*UPh. Besides, the following ligands were located in the crystal structure: glycerol, 1,2-ethanediol, chloride, magnesium, and sodium ions, and bound water molecules. The atomic displacement parameters were refined anisotropically. The validity of the structure refinement was checked with the Coot [24, 25] and MolProbity [26] programs and using the PDB Validation Server (http://validate.rcsb.org). The principal structure-refinement parameters are summarized in Table 1. The structure of the complex was deposited in the Research Collaboratory for Structural Bioinformatics Protein Data Bank RCSB PDB (PDB ID: 6RCA). The 3D structures were drawn with the PyMol program [27].

Classical Molecular Dynamics Simulation

To evaluate the binding stability of ANU to *Vch*UPh, we performed molecular dynamics (MD) simulations of this complex with the GROMACS software package (version 2018.6) [28] in the CHARMM additive all-atom force field [29, 30] using the latest C36m parameters [31]. The ligand models were processed, the partial atomic charges and van-der-Waals parameters were assigned, and the force constants for bonds, valence angles, and dihedral angles were generated using the CGenFF web server [32]. Water molecules were given explicitly and described by the three-site TIP3P model. Long-range electrostatic interactions were calculated by the particle-mesh Ewald (PME) method [23] with a cubic interpolation. Van-der-Waals interactions were described by the smooth force-switch function in the range from 10 to 12 Å. The pressure in the system was controlled with the Parrinello–Rahman barostat [33] at 1 bar. The temperature of the MD system was maintained constant with the V-rescale thermostat [34] at 300 K. Before the MD

simulations, the atomic parameters of the models were optimized using the chosen force field in a virtual cell by the gradient descent method followed by simulations of the system with position restraints on protein and ligand heavy atoms using NVT and NPT ensembles for 200 ps. The MD trajectory was set to 10 ns. Newton's equations of motion were integrated with a step of 2 fs by the leap-frog algorithm [35].

Determination of the Relative Ligand Binding Affinity by the Linear Interaction Energy Method

The relative ligand binding affinity was calculated by the linear interaction energy (LIE) method [36, 37] using the gmx_lie program implemented in the GROMACS package. The average force-field energies of van-der-Waals (E_{vdw}^{solv}) and electrostatic (E_{coul}^{solv}) interactions between the ligand and water in the ligand–water system were calculated during 10-ns MD simulations. The empirical constants α and β characterizing the contributions of the van-der-Waals and electrostatic interactions to the binding energy were chosen as recommended in [37]. For the ligands considered in this work, $\alpha = 0.18$ and $\beta = 0.33$.

Calculation of the Protein–Ligand Binding Free Energy by the Free-Energy Perturbation (FEP) Method

The protein–ligand binding free energy (ΔG_{bind}) was calculated using a thermodynamic cycle described in [38]. In the first step, differences of reduced potencial depending on the Kirkwood coupling parameter (λ parameter [39]) were collected. For the protein–ligand and protein–water systems, MD simulations were performed for 2 ns using the leap-frog algorithm for integrating the Langevin equation for each set of λ parameters. In the case of the protein–ligand system, apart from parameters for Coulomb and van-der-Waals interactions between the ligand and the protein, additional restraints were introduced to keep the ligand in the binding site, the λ parameter being successively varied in the [0–1] range. In the case of the ligand–water system, the coupling parameters were varied only for Coulomb and van-der-Waals interactions between the ligand and water. The correction for the energy of restraints for the ligand–water system, which is required for the evaluation of ΔG_{bind}, was calculated analytically by the formula

$$\Delta G_{rest}^{solv} = -RT \ln\left[\frac{8\pi V_0}{r_A^2 \sin\theta_A \sin\theta_B} \times \frac{\sqrt{K_r K_{\theta_A} K_{\theta_B} K_{\varphi_A} K_{\varphi_B} K_{\varphi_C}}}{(2\pi RT)^3}\right],$$

where r_A is the pseudo-bond length (nm), θ_A, θ_B are angle restraints, K_r, K_{θ_A}, K_{θ_B}, K_{φ_A}, K_{φ_B}, K_{φ_C} are force constants, V_0 is the standard volume (1.66 nm^3), R is the universal gas constant, and T is the temperature

Table 1. X-ray-data collection and processing and the structure solution and refinement statistics

X-ray-data collection	
Synchrotron radiation source, protein crystallography beamline	BESSY, Beamline 14.1
Wavelength, Å	0.886
Detector	PSI PILATUS 6M
Space group	$P3_1$
$a = b$; c, Å	93.25; 152.93
$\alpha = \beta$; γ, deg	90.00; 120.00
$CC_{1/2}$**	99.9 (81.1)*
Resolution range for X-ray data collection, Å	44.60–1.34 (1.43–1.34)*
Total number of reflections	3388833 (515634)*
Number of unique reflections	329624 (52973)*
Completeness of data, %	99.7 (99.0)*
R_{measF}, %	14.7 (127.0)*
Average value $\langle I/\sigma(I)\rangle$	11.52 (1.90)*
Overall Wilson temperature factor, Å^2	16.61
Structure refinement	
Resolution range for refinement, Å	44.59–1.34 (1.36–1.34)*
Cut-off Sigma, min($\sigma(\|F\|/\|F\|$)	1.93
Number of reflections in the working set	329397 (12720)*
Number of reflections in the test set	3456 (135)*
R_{work}, %	13.5 (26.6)*
R_{free}, %	16.9 (29.1)*
Cruickshank DPI, Å	0.04
Number of refined non-hydrogen atoms	
Protein	11480
Inorganic ions	6
Ligands	172
Water	2004
Rms deviation from ideal geometry	
Bond lengths, Å	0.017
Bond angles, deg	1.76
Average B factor for all atoms, Å^2	17.12
Ramachandran statistics	
Number of residues in the most favored regions, %	98.13
Number of residues in the allowed regions, %	1.47
IDPDB	6RCA

* The data for the last high-resolution shell are given in parentheses.

** $CC_{1/2}$ is the Pearson's correlation coefficient between the measured intensities of two randomly assigned half-subsets of reflections in the overall data set.

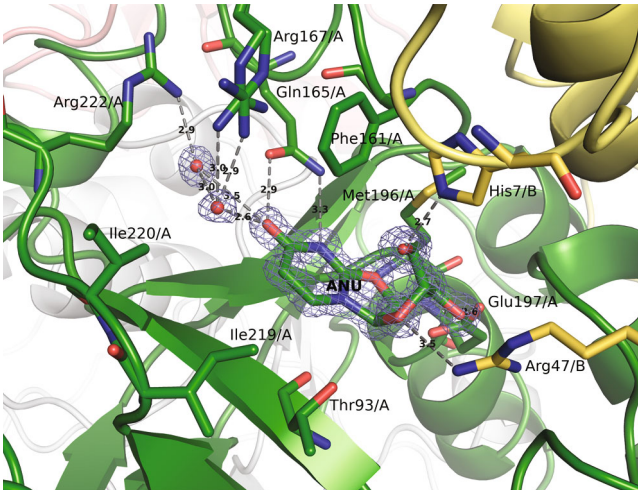

Fig. 2. Three-dimensional organization of the enzyme active site of *Vch*UPh in complex with 2,2'-anhydrouridine (ANU; IDPDB: 6RCA). A fragment of the $2F_o–F_c$ electron density map is shown. Polar contacts between hydrogen-bond donors and acceptors are indicated by dashed lines. Selected residues and secondary structure elements of different subunits of the AB homodimer are shown in different colors.

(K) [40]. For each coupling parameter λ in MD simulations, the geometry was optimized and the system was equilibrated with restraints on positions of non-hydrogen atoms of the protein and the ligand in NVT and NPT ensembles during 100 ps. Long-range Coulomb and van-der-Waals interactions were taken into account by the PME method [23], due to which no additional calculations of the corrections for the effect of long-range interactions were required. The ΔU values, which were saved every 0.02 ps, were processed with the alchemical-analysis program [41] using the multistate Bennett acceptance ratio estimator method [42].

RESULTS AND DISCUSSION

Three-Dimensional Organization of the Enzyme VchUPh in Complex with 2,2'-Anhydrouridine

The structural organization of the enzyme *Vch*UPh in complex with 2,2'-anhydrouridine is similar to that of *Vch*UPh structures reported previously [15, 21, 43]. Each subunit of the biological *Vch*UPh molecule, which exists as a toroidal homohexamer with a diameter of ~106 Å, is composed of 253 residues (the molecular weight is 27.5 kDa). The monomer consists of eight β-strands (28% residues) and eight α-helices (32% residue) assigned with the DSSP program [44]. The interdomain region of each homodimer of the hexamer contains a Na^+ ion coordinated by three pairs of alike residues from adjacent subunits of the homodimer. Each dimer contains two identical active sites formed by residues of both subunits of the homodimer [45–47]. Apart from the binding site, the active site includes the gate loop (L11). In the structure of *Vch*UPh in complex with 2,2'-anhydrouridine, the loop L11 has an open conformation [43] in all subunits of the hexamer.

Active Site in VchUPh Complexed with 2,2'-Anhydrouridine

In the *Vch*UPh molecule, 2,2'-anhydrouridine occupies the whole nucleoside-binding site (Fig. 2). The inhibitor molecules are located in all six active sites of the hexameric UPh molecule. Let us consider the active site of the A subunit of the AB homodimer, the binding site of which contains the ligand at full occupancy. It can be seen that the ANU molecule bound in the active site interacts via hydrogen bonds with the conserved residues of the nucleoside-binding site: NE2_Gln165/A—3.33 Å—N3_ANU; OE1_Gln165/A—2.95 Å—O4_ANU, NE2_His7/B—2.64 Å—O5'_ANU; OE2_Glu197/A—2.56 Å—O3'_ANU, OE1_Glu197/A—3.33 Å—O3'_ANU. There is also a significant electrostatic interaction (3.37 Å) between the N1_ANU atom and the main-chain oxygen atom of Thr93/A, which forms a flexible wall of the active site [21, 43]. Besides, ANU is linked to the residue Arg222 through a water molecule; NH2_Arg222/A —2.88 Å—H_2O—3.49 Å—O4_ANU.

In the structure under consideration, Arg167, being also a key residue for the binding of nucleosides and free heterocyclic bases [21, 43], adopts two alternative conformations (Figs. 2 and 3b) (the occupancies of these positions in the A subunit are 0.53 and 0.47). In both conformations, Arg167 is not directly bound to ANU but is linked to the inhibitor through a structured water molecule: NH2_Arg167/A—3.01 Å—H_2O—2.60 Å—O4_ANU for the A conformation (the occupancy for this confirmation is 0.47) and NH1_Arg167/A—2.85 Å —H_2O—2.60 Å—O4_ANU for the B conformation (the occupancy is 0.53). It is worth noting that this is the first time that the conserved active-site residue, which is linked, although indirectly, to a ligand at full occupancy, adopts two conformations. Besides, the position of the water molecule, through which Arg167 is linked to ANU, is more stable (the occupancy is 1.00; the temperature factor is 24.55 $Å^2$) compared to the positions of the side-chain atoms of Arg167.

The side chain of Met196/A stabilizes the position of the ribose moiety of 2,2'-anhydrouridine via van-der-Waals interactions with atoms of the furanose ring (C1'–C2'–C3'–C4'–O4') (Fig. 2). There is a hydrophobic pocket formed by Ile220 and Ile221 in the vicinity of the carbon atom C5 of the aromatic heterocycle of ANU (Fig. 2).

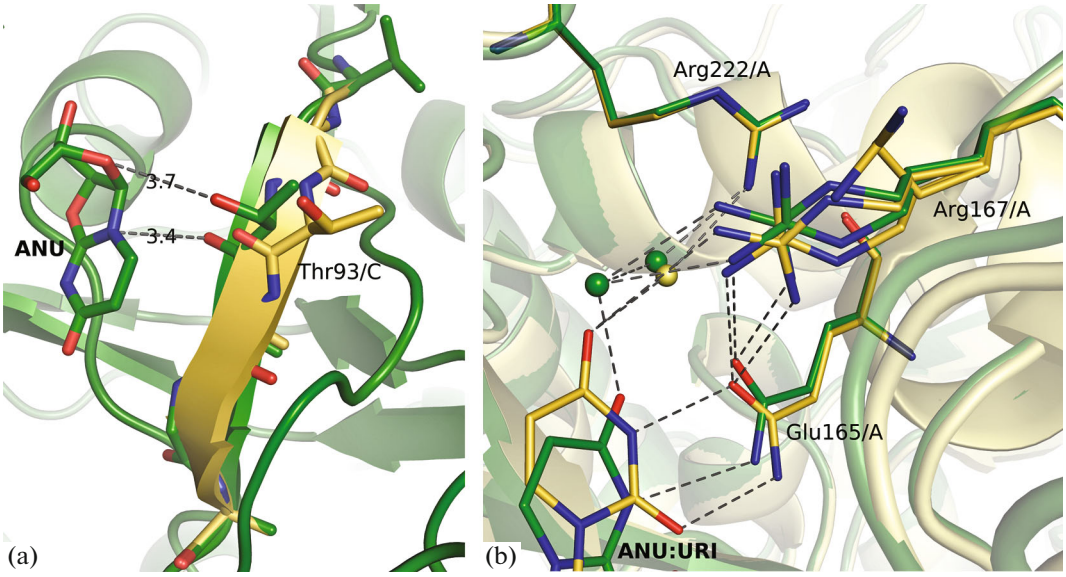

Fig. 3. (a) Alternative conformations of the region (residues 92–95) of the β5 strand of *Vch*UPh in complex with 2,2'-anhydrouridine (ANU); (b) of the residue Arg167/A in the *Vch*UPh complexes with 2,2'-anhydrouridine (dark) and uridine (URI) (light).

Effect of 2,2'-Anhydrouridine Binding on the Conformation of Structurally Functional Elements of VchUPh

Like in the previously considered high-resolution structures of *Vch*UPh in complexes with substrates [43] and the pseudo-substrate (6-methyluracil) [21], there are two conformations of the β5- and β8-strands in the structure of *Vch*UPh complexed with the ligand bound at partial occupancy. Two positions of the secondary structure elements correspond to the ligated and unligated states. In the structure under consideration, ANU molecules are bound in the active sites of the C, D, E, and F subunits at partial occupancy. In these subunits, two conformations are observed for the region composed of the residues 92–95 of the β5-strand (Fig. 3a), which is involved in the formation of the active site, and the parallel region of the β8-strand (residues 217–219). The rms deviation between the atomic coordinates of the residues 92–95 and 217–219 of the C subunit in one of the two positions in the structure under consideration and the corresponding residues of the A subunit of unligated *Vch*UPh (IDPDB: 6EYP, 1.22 Å resolution) is 0.18 Å. The rms deviation between the coordinates of the residues 92–95 and 217–219 in the second positions in the structure under consideration and the corresponding residues of these regions in the structure of the enzyme ligated with the substrate uridine (IDPDB: 5M2T, [43]) is 0.19 Å. The rms deviation between the atomic coordinates of the residues 92–95 and 217–219, which adopt two positions in the C subunit of the structure of *Vch*UPh complexed with ANU, is 0.6 Å. A similar situation is observed for the D, E, and F subunits. Therefore, two conformations of the β5- and β8-strands may be indicative of the limiting positions of these structural elements of *Vch*UPh during the binding of the inhibitor to the enzyme. The displacement of the β5-strand is apparently attributed to a weak hydrogen bond and electrostatic interactions of the atoms of the inhibitor with both the backbone and the side chain of Thr93 (O_Thr93/C—3.38 Å—N1_ANU; OG1_Thr93—3.70 Å—O4') (Fig. 3a).

Comparison of the Structures of VchUPh in Complexes with 2,2'-Anhydrouridine and Uridine

A comparison of the binding sites in the structures of *Vch*UPh complexed with uridine [42] (IDPDB: 5M2T; the B subunit, the occupancy of URI is 1.00) and 2,2'-anhydrouridine (IDPDB: 6RCA; the A subunit) shows that the rms deviation between the coordinates of the backbone atoms of the nucleoside-binding site residues in these complexes is 0.60 Å; the rms deviation between the coordinates of the side-chain atoms is 0.71 Å. The largest differences are observed for the positions and conformations of the residues Thr93 and Phe6 involved in the environment of the ligand (ANU or URI).

A comparison of the atomic coordinates of Thr93 involved in the ribose-binding subsite of the active site shows that this residue is ~0.5 Å closer to the ligand in the structure of *Vch*UPh complexed with uridine [43] than in the structure of *Vch*UPh in complex with ANU. Therefore, the active site in the structure of *Vch*UPh complexed with uridine is more compact compared to the *Vch*UPh + ANU structure. Although the residue Phe6 of the adjacent subunit is not involved in the binding sites of *Vch*UPh, it is located in the immediate vicinity to His8 involved in the ribose-binding subsite of the active site. The bulky phenyl side

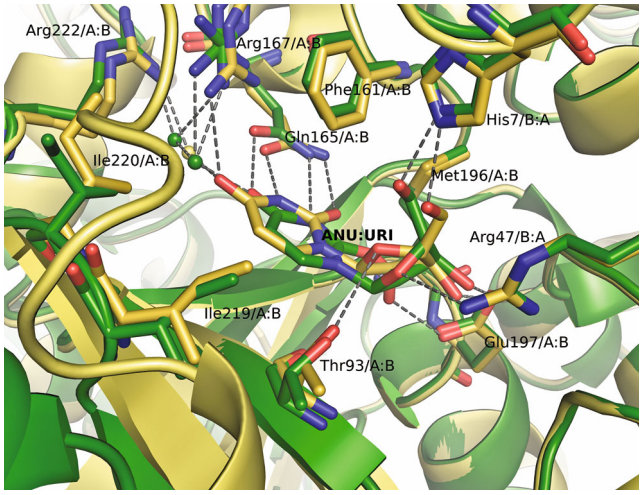

Fig. 4. Superposition of the active sites in the structures of *Vch*UPhc in complexes with 2,2'-anhydrouridine (IDPDB: 6RCA, ANU) and uridine (IDPDB: 5M2T; URI).

chain of Phe6 may restrict the access of ligands to the active site of the enzyme. Apparently, the difference in the position of the side chain of Phe6 in the complexes of *Vch*UPh with ANU and URI (the rms deviation of the atomic coordinates is 3.61 Å) is due to van-der-Waals interactions with the side-chain atoms of Ile227 of the gate loop L11 [21, 43]. In the structure of *Vch*UPh complexed with uridine, the loop L11 in the B subunit is in a closed conformation as opposed to the structure of *Vch*UPh in complex with the inhibitor.

The main difference in the system of hydrogen bonds formed by the ligands (Fig. 4) is mainly determined by the configuration of the ligands (uridine and 2,2'-anhydrouridine) and the relative arrangement of their functional groups with respect to the active-site residues. The rms deviation between the atomic coordinates of all corresponding atoms of uridine and 2,2'-anhydrouridine is 1.01 Å; between the atomic coordinates of the pyrimidine and ribose moieties, 1.11 and 0.80 Å, respectively. The furanose ring in the uridine molecule adopts the strained twist conformation C1'-endo/O4'-exo [42], whereas this ring in the ANU molecule has the envelope conformation C4'-exo. Therefore, the uridine molecule adopts a high-energy conformation due to the deformation caused by the binding-site residues [43]. Besides, due to an additional O2–C2' covalent bond, ANU is more rigid than the uridine molecule. In contrast to uridine, the N3 atom of 2,2'-anhydrouridine does not form a hydrogen bond with the side-chain atom OE1 of Gln165; the distances between these atoms in all ligated subuntis are longer than 3.40 Å. This is attributed to another arrangement of the pyrimidine ring in the 2,2'-anhydrouridine molecule compared to uridine. Besides, the 2,2'-anhydrouridine molecule, unlike uridine, does not form a stable hydrogen bond with the conserved residue Arg167 that is involved in the uracil-binding subsite of the active site; instead ANU is linked to this residue through a structured water molecule (Fig. 4).

There are also differences in the ligand binding to the ribose-binding subsite of the active site of *Vch*UPh. The residue Glu197 forms hydrogen bonds with the hydroxyl oxygen atoms O2' and O3' of the ribose moiety of uridine (OE1_Glu197/B—2.66 Å—O2'_URI, OE1_Gln197/B—3.10 Å—O3'_URI, OE2_Gln197/B—2.70 Å—O3'_URI), whereas this residue forms a hydrogen bond only with the hydroxyl oxygen atom O3' of 2,2'-anhydrouridine (OE2_Glu197/A—2.56 Å—O3'_ANU, OE1_Glu197/A—3.33 Å—O3'_ANU). The hydroxyl oxygen atom O2' of uridine interacts also with the backbone nitrogen atom of Met196 (N_Met196/B—3.00 Å—O2'_URI). The hydroxyl group O2' is absent in the inhibitor, and the oxygen atom O2' is involved in the alkoxy group, which does not form hydrogen bonds with the protein molecule and, apparently, only electrostatically interacts with the backbone nitrogen atom of Met196 (N_Met196/A—3.42 Å—O2'_ANU).

The 2,2'-anhydrouridine molecule forms a smaller number of stable hydrogen bonds with the active site of the enzyme, and these hydrogen bonds are, on the whole, longer compared to those in the complex with uridine. This fact, the open conformation of the gate loop L11, and the less compact arrangement of the walls of the active site are indicative of a lower enthalpy of inhibitor binding compared to the enthalpy of binding of the native substrate uridine. Besides, the 2,2'-anhydrouridine molecule is more rigid than uridine, which decreases the entropy component of the binding free energy.

The residue Arg167 of the B subunit in the structure of *Vch*UPh complexed with uridine adopts a single conformation. However, the side chain of Arg167 in the A subunit adopts three alternative conformations (the occupancies are 0.44, 0.33, and 0.23). In the active site of the A subunit, uridine is bound at partial occupancy (0.75) as opposed to the active site of the B subunit. Therefore, it can be considered that Arg167 is in the ligand-free state in 25% of the subunits. Apparently, there is a relationship between the mobility of the side chain of Arg167 and its binding to the ligand. Thus, the side chain of this residue is more flexible in the free state than in the state hydrogen-bonded to the ligand atoms.

Molecular dynamics simulations showed that the native substrate uridine is stronger bound to *Vch*UPh compared to the inhibitor. The average rms deviation of the coordinates of the non-hydrogen atoms of uridine from the initial position during the 10-ns trajectory is 0.97 Å ($\sigma = 0.16$ Å); of the non-hydrogen atoms of 2,2'-anhydrouridine, 2.44 Å ($\sigma = 0.55$ Å) (Table 2). Besides, during the MD trajectory, uridine forms, on the average, a much larger number of hydrogen bonds (4.39) with the residues of *Vch*UPh compared to 2,2'-

Table 2. Molecular dynamics study of the protein–ligand complexes

Complex	*Vch*UPh + ANU	*Vch*UPh + URI
Average root-mean-squared deviation of atomic coordinates of the ligand from the initial position, Å	2.44 ± 0.55	0.97 ± 0.16
Root-mean-squared deviation of the distance between the centers of mass of the protein–ligand complex, Å	0.47	0.25
Average number of protein–ligand hydrogen bonds	0.76 ± 0.94	4.39 ± 0.77
Relative ligand binding affinity calculated by the linear interaction energy method		
E_{vdw}^{solv}, kJ/mol	−66.8	−67.5
E_{coul}^{solv}, kJ/mol	−191.9	−257.9
ΔG_{bind}, kJ/mol	−5.8	−14.8
ΔG_{bind} of the protein–ligand complex calculated by the free-energy perturbation method		
$\Delta G_{vdw+coul}^{solv}$, kJ/mol	71.518 ± 0.450	103.835 ± 0.722
ΔG_{rest}^{solv}, kJ/mol	29.969	30.078
$\Delta G_{vdw+coul+rest}^{prot}$, kJ/mol	134.404 ± 0.793	147.205 ± 1.077
ΔG_{bind}, kJ/mol	−32.917 ± 0.912	−13.292 ± 1.297

anhydrouridine (0.76), which is in agreement with the X-ray diffraction data for the complexes. The 2,2'-anhydrouridine and uridine molecules remain in the active site throughout the MD simulation. The relative binding affinity of uridine to the protein (ΔG_{bind}) calculated by the LIE method is ~2.6 times higher than ΔG_{bind} for 2,2'-anhydrouridine (Table 2).

The protein–ligand binding free energy calculated by the more precise [36, 37] but more time-consuming free-energy perturbation method is −13.292 ± 1.297 and −32.917 ± 0.912 kJ/mol per active site of the enzyme for uridine and 2,2'-anhydrouridine, respectively (Table 2). It should be noted that the protein–ligand binding free energy ($\Delta G_{vdw+coul+rest}^{prot}$) for the inhibitor is lower than that for the substrate. This is indicative of the lower enthalpy of inhibitor binding, but the difference in the solvation energy of the inhibitor and the substrate is larger than the difference in $\Delta G_{vdw+coul+rest}^{prot}$. Hence, despite the smaller number of hydrogen bonds, the binding of the inhibitor (2,2'-anhydrouridine) to the active site of *Vch*UPh is energetically more favorable than the binding of the native substrate uridine. The inhibition constant K_i calculated from the binding free energy of 2,2'-anhydrouridine ($K_i = e^{(\Delta G/RT)}$) is 1.9 μM per active site; the inhibition constant for six active sites K_i = 11.4 μM, which is of the same order of magnitude as the experimental data for similar *E. coli* uridine phosphorylase [7]. The LIE method proved to be not applicable to the protein–ligand system apparently because of high mobility of 2,2'-anhydrouridine in the active site of the enzyme compared to uridine and also due to the use of empirical constants, which are difficult to correctly choose without additional studies.

It is worth noting that the protein–ligand binding free energy for the native substrate uridine is relatively low. Apparently, the low protein–ligand binding free energy per active site is in vivo compensated by the multimeric structure of bacterial UPhs.

Comparison of the Structures of VchUPh and StUPh in Complexes with 2,2'-Anhydrouridine

We compared highly conserved binding sites in the structures of the complexes of *Salmonella typhimurium* uridine phosphorylase *St*UPh + ANU (IDPDB: 3FWP) and *Vch*UPh + ANU (IDPDB: 6RCA). The rms deviation between the coordinates of all atoms of the active-site residues is 0.20 Å; between the coordinates of atoms of ANU in the binding sites, 0.26 Å. The largest deviations are observed for the oxygen atom O4_ANU (0.55 Å) and the N3 and C4 atoms of the pyrimidine ring (0.33 and 0.26 Å, respectively). The difference in the position of the ANU molecule in the binding sites of the *Vch*UPh and *St*UPh structures is apparently attributed to the fact that ANU located in the active site of *Vch*UPh forms an additional interaction to the water molecule hydrogen-bonded to the residue Arg167 (O4_ANU—2.68 Å—H_2O—2.88 Å—NH2_Arg167). The rather bulky phosphate ion bound in the phosphate-binding site in the structure of *St*UPh complexed with ANU and phosphate (3FWP) may prevent the ANU molecule from penetrating deeper in the active site of the enzyme. However, this hypothesis was not supported by the structure of *St*UPh in complex with ANU determined at 2.36 Å resolution (IDPDB: 3C74) (Fig. 5b). In the latter structure, like in the structure of *Vch*UPh complexed with ANU, none of the active sites contains orthophosphate. The position and conformation of the

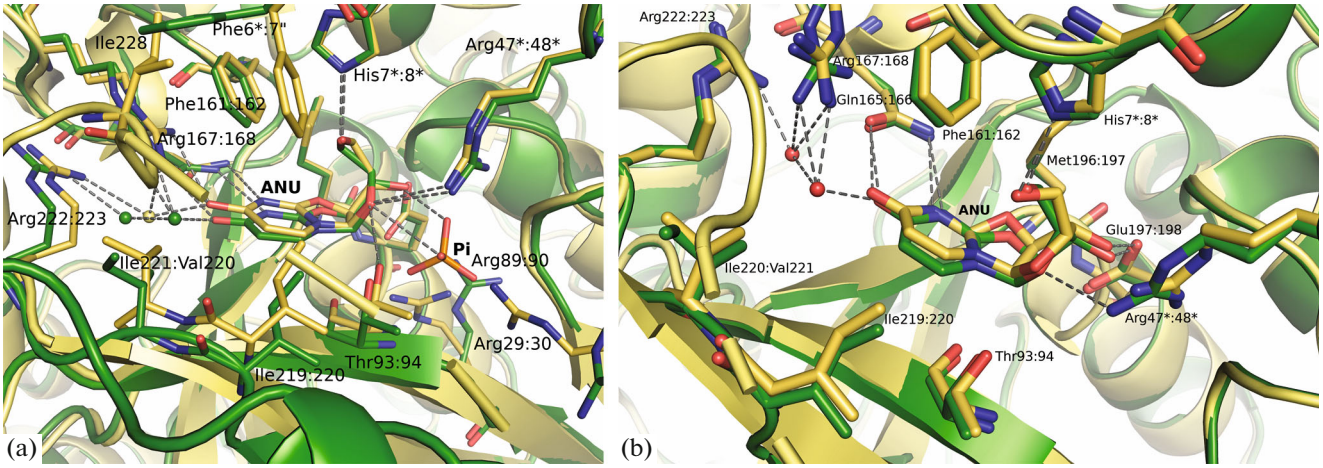

Fig. 5. Superposition of the active-site residues of *Vch*UPh in complex with 2,2'-anhydrouridine (IDPDB: 6RCA; ANU, dark) and the active-site residues of two complexes of uridine phosphorylase *St*UPh: (a) *St*UPh in complex with 2,2'-anhydrouridine and a phosphate ion (P*i*) (IDPDB: 3FWP; 1.86 Å resolution, the active site of the BD homodimer, light-colored); (b) *St*UPh in complex with 2,2'-anhydrouridine (IDPDB: 3C74; 2.36 Å resolution, the active site of the BD homodimer, light-colored). The residues of the subunit, which makes a smaller quantitative contribution to the binding-site formation, are indicated by an asterisk (B for *Vch*UPh, D for *St*UPh).

inhibitor in the *St*UPh complex with ANU are much similar to those in the complex 3FWP, which is ligated by both ANU and phosphate, than to those in the *Vch*UPh complex with ANU (Fig. 5b).

CONCLUSIONS

The inhibitor 2,2'-anhydrouridine is located in all nucleoside-binding subsites of six identical active sites of uridine phosphorylase from *Vibrio cholerae*.

A comparison of the binding sites in the structures of *Vch*UPh complexed with 2,2'-anhydrouridine and uridine shows that the largest differences are observed in the positions and conformations of the residues Thr93 and Phe6 coordinated to the ligands. The residue Thr93 is ~0.5 Å closer to the ligand in the structure of *Vch*UPh complexed with uridine than in the structure of *Vch*UPh with ANU. Therefore, the active site in *Vch*UPh complexed with uridine is more compact than that in the *Vch*UPh + ANU structure. The difference in the position of the side chain of Phe6 in the structures of *Vch*UPh complexed with ANU and URI is due to the van-der-Waals interaction with the side chain of Ile227 of the gate loop L11. The loop L11 adopts different conformations in these complexes. In the *Vch*UPh complex with ANU, this loop has an open conformation, whereas it is in a closed conformation in the complex with uridine. The 2,2'-anhydrouridine molecule forms a smaller number of stable hydrogen bonds with the active site of the enzyme and these bonds are longer compared to the native substrate uridine. This fact, the open conformation of the gate loop, and the less compact arrangement of the walls of the active site are responsible for the lower enthalpy of inhibitor binding compared to the enthalpy of binding of the native substrate uridine. Besides, the 2,2'-anhydrouridine is more rigid than uridine, which decreases the entropy component of the binding free energy

Molecular dynamics simulations demonstrated that the binding of the native substrate uridine to *Vch*UPh is stronger than the binding of the inhibitor. However, the protein–ligand binding free energy calculated by the free-energy perturbation method is -13.292 ± 1.297 and -32.917 ± 0.912 kJ/mol per active site of the enzyme for uridine and 2,2'-anhydrouridine, respectively. The protein–ligand binding free energy for the inhibitor is lower than that for the substrate, which is indicative of the lower enthalpy of inhibitor binding, but the difference in the solvation energy of the inhibitor and the substrate is much larger than the difference in the protein–ligand binding free energy. Hence, despite the smaller number of hydrogen bonds, the binding of the inhibitor (2,2'-anhydrouridine) to the active site of *Vch*UPh is energetically more favorable than the binding of the native substrate uridine.

ACKNOWLEDGMENTS

The calculations were performed by Hybrid high-performance computing cluster of FRC CS RAS [48].

FUNDING

This work was supported by the Ministry of Science and Higher Education within the State assignment FSRC "Crystallography and Photonics" RAS.

REFERENCES

1. K. Katsumata, H. Tomioka, T. Sumi, et al., Cancer Chemother Pharmacol. **51**, 155 (2003).
2. P. J. Finan, P. A. Koklitis, E. M. Chisholm, et al., Br. J. Cancer **50**, 711 (1984).
3. A. Leyva, I. Kraal, J. Lankelma, et al., Anticancer Res. **3**, 227 (1983).
4. A. Kanzaki, Y. Takebayashi, H. Bando, et al., Int. J. Cancer **97**, 631 (2002).
5. C. Luccioni, J. Beaumatin, V. Bardot, et al., Int. J. Cancer **58**, 517 (1994).
6. M. H. el Kouni, F. N. Naguib, J. G. Niedzwicki, et al., J. Biol. Chem. **263**, 6081 (1988).
7. A. K. Drabikowska, L. Lissowska, Z. Veres, et al., Biochem. Pharmacol. **36**, 4125 (1987).
8. Z. Veres, A. Neszmelyi, A. Szabolcs, et al., Eur. J. Biochem. **178**, 173 (1988).
9. S. Watanabe, A. Hino, K. Wada, et al., J. Biol. Chem. **270**, 12191 (1995).
10. M. H. el Kouni, F. N. Naguib, S. H. Chu, et al., Mol. Pharmacol. **34**, 104 (1988).
11. F. N. Naguib, J. G. Niedzwicki, M. H. Iltzsch, et al., Leuk. Res. **11**, 855 (1987).
12. A. A. Lashkov, N. E. Zhukhlistova, S. E. Sotnichenko, et al., Crystallogr. Rep. **55** (1), 41 (2010).
13. A. A. Lashkov, N. E. Zhukhlistova, A. G. Gabdoulkhakov, et al., Acta Crystallogr. D **66**, 51 (2010).
14. V. I. Timofeev, A. A. Lashkov, A. G. Gabdoulkhakov, et al., Acta Crystallogr. F **63**, 852 (2007).
15. A. A. Lashkov, A. G. Gabdulkhakov, I. I. Prokofev, et al., Acta Crystallogr. F **68**, 1394 (2012).
16. I. I. Prokofev, A. A. Lashkov, A. G. Gabdulkhakov, et al., Acta Crystallogr. F **70**, 60 (2014).
17. M. Zolotukhina, I. Ovcharova, S. Eremina, et al., Res. Microbiol. **154**, 510 (2003).
18. W. Kabsch, Acta Crystallogr. D **66**, 125 (2010).
19. A. J. Mccoy, R. W. Grosse-Kunstleve, P. D. Adams, et al., J. Appl. Crystallogr. **40**, 658 (2007).
20. A. J. McCoy, Acta Crystallogr. D **63**, 32 (2007).
21. I. I. Prokofev, A. A. Lashkov, A. G. Gabdulkhakov, et al., Crystallogr. Rep. **63** (3), 418 (2018).
22. P. D. Adams, P. V. Afonine, G. Bunkoczi, et al., Acta Crystallogr. D **66**, 213 (2010).
23. P. V. Afonine, R. W. Grosse-Kunstleve, N. Echols, et al., Acta Crystallogr. D **68**, 352 (2012).
24. P. Emsley and K. Cowtan, Acta Crystallogr. D **60**, 2126 (2004).
25. P. Emsley, B. Lohkamp, W. G. Scott, et al., Acta Crystallogr. D **66**, 486 (2010).
26. I. W. Davis, A. Leaver-Fay, V. B. Chen, et al., Nucleic Acids Res. **35**, 375 (2007).
27. W. L. DeLano, Abstr. Pap. Am. Chem. Soc. **228**, 313 (2004).
28. D. Van Der Spoel, E. Lindahl, B. Hess, et al., J. Comput. Chem. **26**, 1701 (2005).
29. A. D. MacKerell, D. Bashford, M. Bellott, et al., J. Phys. Chem. B **102**, 3586 (1998).
30. A. D. MacKerell, Abstr. Pap. Am. Chem. Soc. **216**, 696 (1998).
31. J. Huang, S. Rauscher, G. Nawrocki, et al., Nat. Methods **14**, 71 (2016).
32. K. Vanommeslaeghe, E. Hatcher, C. Acharya, et al., J. Comput. Chem. **31**, 671 (2010).
33. M. Parrinello and A. Rahman, J. Appl. Phys. **52**, 7182 (1981).
34. G. Bussi and M. Parrinello, Comput. Phys. Commun. **179**, 26 (2008).
35. B. J. Leimkuhler, S. Reich, and R. D. Skeel, *Mathematical Approaches to Biomolecular Structure and Dynamics,* Ed. by J. P. Mesirov et al., *The IMA Volumes in Mathematics and Its Applications,* Vol. 82 (Springer, New York, 1996), p. 161.
36. J. Aqvist and J. Marelius, Comb. Chem. High Throughput Screening **4**, 613 (2001).
37. T. Hansson, J. Marelius, and J. Aqvist, J. Comput. Aided Mol. Des. **12**, 27 (1998).
38. M. Aldeghi, A. Heifetz, M. J. Bodkin, et al., Chem. Sci. **7**, 207 (2016).
39. J. Kirkwood, J. Chem. Phys. **3**, 300 (1935).
40. S. Boresch, F. Tettinger, M. Leitgeb, et al., J. Phys. Chem. B **107**, 9535 (2003).
41. P. V. Klimovich and D. L. Mobley, J. Comput. Aided Mol. Des. **29**, 1007 (2015).
42. M. R. Shirts and J. D. Chodera, J. Chem. Phys. **129**, 124105 (2008).
43. I. I. Prokof'ev, A. G. Gabdulkhakov, V. V. Balaev, et al., Crystallogr. Rep. **61**, 954 (2016).
44. W. G. Touw, C. Baakman, J. Black, et al., Nucl. Acids Res. **43**, 364 (2015).
45. T. T. Caradoc-Davies, S. M. Cutfield, I. L. Lamont, et al., J. Mol. Biol. **337**, 337 (2004).
46. A. A. Lashkov, N. E. Zhukhlistova, A. H. Gabdoulkhakov, et al., Acta Crystallogr. D **66**, 51 (2010).
47. A. M. Mikhailov, E. A. Smirnova, V. L. Tsuprun, et al., Biochem. Int. **26**, 607 (1992).
48. Federal Research Center Computer Science and Control of Russian Academy of Sciences. Available at http://hhpcc.frccsc.ru

Translated by T. Safonova